Materials Letters 227 (2018) 141–144

Contents lists available at ScienceDirect

Materials Letters

journal homepage: www.elsevier.com/locate/mlblue

Featured Letter

Tip radius variation with elastic indentation depth

Alan F. Jankowski [a,*], H.S. Tanvir Ahmed [b], Eric M. Brannigan [c]

[a] Sandia National Laboratory, P.O. Box 969 MS-9161, Livermore, CA 94551-0969, United States
[b] Intel Corporation, 2501 NW Butler St., Portland, OR 97124, United States
[c] Los Alamos National Laboratory, P.O. Box 1663, Los Alamos, NM 87545, United States

ARTICLE INFO

Article history:
Received 8 January 2018
Received in revised form 21 March 2018
Accepted 9 May 2018

Keywords:
Nanoindentation
Indenter tip radius
Reduced modulus
Tapping mode

ABSTRACT

The reduced elastic modulus of a material is measured with a nanoindenter probe that is operated in the tapping mode. The resonant frequency of a freely oscillating cantilever is reduced when contact is made between the indenter tip and surface under investigation. It's shown using elasticity theory that the elastic deformation is a function of the indenter tip radius. A deeper penetration within the elastic range can change the tip radius, and introduce an error of 10% in calculating the reduced elastic modulus.

1. Introduction

A series of known materials are analyzed in the tapping mode to relate the square of the change in resonant frequency $\mathbf{\Delta f}$ (Hz) of the indenter with displacement $\mathbf{x}$. Once contact is made between the surface and indenter (as seen in Fig. 1), a nonlinear increase in $(\mathbf{\Delta f})^2$ is found with increasing displacement $\mathbf{x}$ until a range of linear elastic response is reached where the amplitude of the oscillation is reduced to just a few nanometers. The elastic range $\mathbf{z}$ (nm) within the displacement $\mathbf{x}$ is found [1–8] where the parameter $\boldsymbol{\alpha}^2$ represents the slope of the variation of $(\mathbf{\Delta f})^2$ with $\mathbf{z}$, i.e. $\boldsymbol{\alpha}$ equals $(\mathbf{\Delta f})\cdot\mathbf{z}^{-1/2}$. The parameter $\boldsymbol{\alpha}$ (Hz·nm$^{-0.5}$) is a power-law function of the reduced elastic modulus $\mathbf{E}^*$ (GPa) for the material, i.e. $\boldsymbol{\alpha}$ equals $c_\alpha\cdot(\mathbf{E}^*)^n$ where c_α is a constant.

The $\boldsymbol{\alpha}$-values measured for known materials are unique to each probe assembly, i.e. the indenter tip mounted to a rigid cantilever support. Calibration measurements of $\boldsymbol{\alpha}$-values with known modulus values of E^*_{ref} for reference materials enables the determination of unknown E^* for materials under study. Relationships are now developed to fit the value of the indenter tip radius $\mathbf{R}$ as a function of elastic deformation $\mathbf{z}$, i.e. $\mathbf{R}(\mathbf{z})$. It's anticipated that more compliant materials have a greater range of elastic deformation, and that at these greater elastic depths of deformation the indenter tip radius will increase due to deformation of the tip and/or a change in the tip shape. It may not be possible to distinguish the different causes for the radius increase, i.e. deformation-induced or natural changes in tip shape.

2. Experimental method and results

Elasticity theory is used in the development of the model [8,9] for the indenter tip radius $\mathbf{R}$ (nm) variation with measured values of $\mathbf{\Delta f}$ and $\mathbf{z}$. The derivation uses Hertz contact mechanics with formulations for the dynamic equivalent of the cantilever with a probe tip. A simplified expression is determined using the first two terms in a Taylor series expansion of the change of frequency $\mathbf{\Delta f}$ for the state of natural oscillation to the contact state with the surface. The tip radius $\mathbf{R}$ is first approximated [8] as computed from the measured $\boldsymbol{\alpha}$-value and the known reduced modulus E^* for the material as

$$\alpha = \left(f_o \times \mathbf{R_o}^{1/2} \times k_c^{-1}\right) \times \mathbf{E}^* \quad (1)$$

The cantilever spring constant k_c equals 22.229 kN·m^{-1} and the resonant frequency constant f_o equals 14.000 kHz. The variation in the data for the measured elastic displacement $\mathbf{z}$ with tip radius $\mathbf{R}$, as computed using Eq. (1), is fit in Fig. 2 with an exponential function as

$$\mathbf{R_z} = c_r \times e^{(c_{rz} \times \mathbf{z})} \quad (2)$$

The curve fit using Eq. (2) now establishes the functional relationship for tip radius variation with elastic deformation.

For Eq. (2), it's found that c_r equals 1.564 nm and c_{rz} equals 0.669 nm^{-1}. The intercept value at zero elastic depth provides

* Corresponding author.
E-mail address: afjanko@sandia.gov (A.F. Jankowski).

https://doi.org/10.1016/j.matlet.2018.05.045
0167-577X/

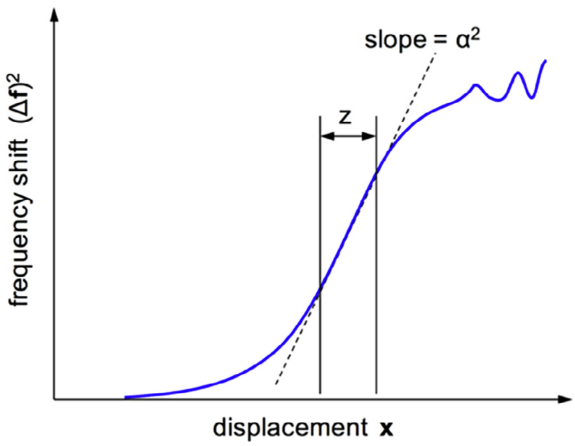

Fig. 1. The resonant frequency shift Δf for a cantilever with a tip in contact with a surface is shown as a function of tip displacement **x**.

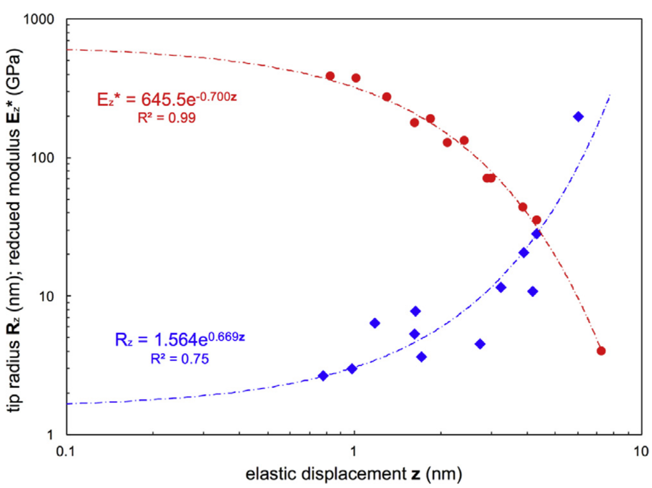

Fig. 2. The variation of the reduced elastic modulus E_z^* (GPa) (circles) and indenter tip radius $\mathbf{R_z}$ (nm) (diamonds) with the elastic displacement **z** (nm).

the undeformed condition for the tip radius as a value of 1.56 nm. A more exact analytic expression than represented in Eq. (1) is next developed [8] that accommodates the nonlinear relationship between α and E*. An additional term is introduced from the Taylor's series expansion of the frequency shift **Δf**. Since the α-values are experimentally determined for materials with known reduced-modulus value E*, the elastic deformation **z** can now be modeled using the more accurate expression

$$\mathbf{E_z}^* = \left\{1 - \left[1 - \left(2\mathbf{a} \times \mathbf{z}^{1/2} \times f_o^{-1}\right)\right]^{1/2}\right\} \times \left[k_c \times (\mathbf{R_z} \times \mathbf{z})^{-1/2}\right] \quad (3)$$

The value for $\mathbf{R_z}$ fitted from Eq. (2) is used as input into Eq. (3). This value for **R** is determined by computing a value of **z** using Eq. (3) to reproduce the known reduced modulus $\mathbf{E}^*_{ref}$ of the indented material. The reference values determined for the elastic moduli [8–15] of each calibration material are listed in Table 1.

The results for the variation of reduced modulus with elastic depth that are plotted in Fig. 2 follow a negative exponential relationship of the form

$$\mathbf{E_z}* = c_e \times e^{-(c_{ez} \times \mathbf{z})} \quad (4)$$

The curve fitting using Eq. (3) establishes the functional relationship for the reduced modulus variation with elastic deformation in Eq. (4) where c_e equals 645 GPa and c_{ez} equals 0.700 nm^{-1}. The E^*_o intercept value is the reduced modulus value at zero elastic depth. The c_e value is that which would be approximated for the E* of the diamond indenter itself. A 645 GPa value for c_e is consistent with the reduced modulus E*, i.e. $(1 - \boldsymbol{\nu}^2)/\mathbf{E}$ value of 0.00078 GPa^{-1}, as is typically reported [8,9] for diamond.

The fitted value for the elastic deformation **z** computed using Eq. (3) versus that value of **z** determined from experimental measurements are listed in Table 1, and plotted in Fig. 3 along with the **R**-values computed using Eqs. (1)-(2). The **z**- and **R**-values computed using these methods [8–16] are consistent in magnitude as seen in the linear curves of Fig. 3.

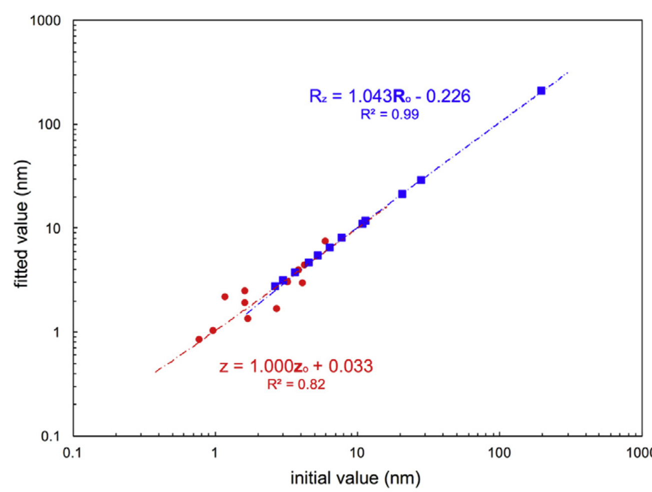

Fig. 3. The variation between experimental and fitted values of **z** (circles), and the values for tip radius **R** using the simplified and expanded Taylor's series formulations (squares).

Table 1
Values of **α**, elastic displacement **z**, Poisson's ration **ν**, reduced elastic modulus **E***, and indenter tip radius **R**.

Sample	α_{meas} ($Hz \cdot nm^{-0.5}$)	z_{meas} (nm)	$z_{eqn.(3)}$ (nm)	R_o (nm)	R_z (nm)	E^*_{ref} (GPa)	E_z^* (GPa)	ν
sapphire poly	401 ± 26	0.98	1.02	3.01	3.09	367.3	367.4	0.27
sapphire (00.2)	392 ± 27	0.78	0.83	2.66	2.73	381.8	381.9	0.27
nickel (111)	325 ± 20	1.71	1.31	3.67	3.76	269.1	269.6	0.31
tantalum (110)	271 ± 23	1.62	1.86	5.29	5.43	186.9	187.1	0.34
silicon (111)	236 ± 23	2.74	1.63	4.55	4.65	175.9	175.9	0.27
vanadium (110)	228 ± 22	1.63	2.43	7.74	7.95	130.4	130.3	0.37
silicon (100)	202 ± 16	1.18	2.13	6.38	6.50	127.1	127.2	0.27
fused quartz	149 ± 13	3.25	3.01	11.49	11.71	70.0	70.0	0.17
fused silica	145 ± 14	4.17	2.92	10.88	11.03	70.0	70.1	0.17
neodymium poly	125 ± 11	3.9	3.88	20.61	20.96	43.6	43.6	0.28
bismuth poly	117 ± 9	4.3	4.35	28.29	28.69	35.0	35.0	0.33
polycarbonate	35.8 ± 1.4	6.08	7.30	198.0	206.4	4.0	4.0	0.37